A Study of Linear Friction Weld Microstructure in Single Crystal CMSX-486 Superalloy

O.T. OLA, O.A. OJO, P. WANJARA, and M.C. CHATURVEDI

The microstructure of linear friction welds in single crystal (SX) CMSX 486 superalloy was studied. Gleeble thermomechanical simulation of the welding process was also performed in order to understand the microstructural changes induced in the alloy during the joining process. Microstructural analysis of the welded and Gleeble-simulated specimens showed that extensive liquation occurred in the alloy during joining, which is in contrast to the general assumption that linear friction welding (LFW) occurs exclusively in the solid state. The study revealed the application of the compressive load during the forging stage of LFW induced rapid solidification of the resultant metastable liquid phase. Nevertheless, part of the liquid resulted in a continuous Hf-base oxide phase along the weld line. Possible ways of preventing the formation of the potentially deleterious oxide film and, thus, improve the prospect of applying LFW for the joining of CMSX-486 superalloy are suggested.

DOI: 10.1007/s11661-011-0928-0

I. INTRODUCTION

HIGHER operating temperature demands on aero-engine components have led to an extensive use of single crystal (SX) nickel-base superalloys in the aerospace industry over the past decade. CMSX-4, a SX nickel-base superalloy, has been successfully used in numerous aero and industrial gas turbine applications.[1] It exhibits superior elevated temperature performance compared to conventionally cast nickel-base superalloys not only because of its higher volume fraction and better stability of the main strengthening phase, γ' precipitates, but also owing to the improved creep properties of SX alloys due to the absence of high-angle grain boundaries. Nevertheless, the alloy does contain grain boundaries with misorientation in the range of 12 to 15 deg, which are on the border between low- and high-angle boundaries and form during the SX directional solidification process. Consequently, in order to improve high-temperature mechanical properties of materials containing these defects, the addition of grain boundary strengthening elements C, B, Hf, and Zr to the CMSX-4 was used to produce a new SX nickel-base superalloy that is known as CMSX-486.[1,2]

There is usually a need for joining turbine parts made of SX superalloys, economically, by the use of various welding techniques during fabrication and repair. However, a study performed on weldability of CMSX-486 superalloy by a conventional fusion welding technique revealed that the alloy is susceptible to fusion zone solidification cracking.[3] The formation of weld fusion zone solidification cracks was also observed in other SX nickel-base superalloys.[4–6] In order to avoid solidification cracking in superalloys, a recent trend in joining crack susceptible materials involves the use of friction welding processes, such as the linear friction welding (LFW) process. LFW makes use of heat generated by a reciprocating linear motion of two work pieces against each other in plasticizing and subsequently joining them under the influence of an axial compressive forging force that is applied during the terminal stage of the process.[7] This process is a state-of-the-art technique with a potential for producing crack-free welds in crack-susceptible superalloys. Therefore, the objective of this research was to study the feasibility of joining SX nickel-base CMSX 486 superalloy by using the LFW process, and to analyze the microstructural changes induced in the alloy by the welding process, which can aid the optimization of the welding process for the alloy.

II. EXPERIMENTAL PROCEDURE

Cast CMSX-486 superalloy with a nominal chemical composition of (wt pct) Ni-9.3Co-5Cr-0.7Mo-8.6W-5.7Al-4.5Ta-1.2Hf-3Re-0.7Ti-0.005Zr-0.07C-0.015B, which was received in the form of rods with dimensions 12-mm diameter and 200-mm length, was used in this work. Linear friction welding test coupons of 17 mm in length were produced by sectioning the as-received material transverse to the solidification direction [001] by using a Hansvedt model DS-2 traveling wire electro-discharge machine (Hansvedt/Arrow EDM, Rantoul, IL). These were then ground to achieve approximately 11-mm width and 11-mm thickness, as schematically represented in Figure 1. The welding test coupons were

O.T. OLA, Doctoral Student, O.A. OJO, Associate Professor, and M.C. CHATURVEDI, Distinguished Professor Emeritus, are with the Department of Mechanical and Manufacturing Engineering, University of Manitoba, Winnipeg, MB R3T 5V6, Canada. Contact e-mail: ojo@cc.umanitoba.ca P. WANJARA, Project Leader and Group Leader, is with the National Research Council Canada, Institute for Aerospace Research, Aerospace Manufacturing Technology Centre, Montréal, PQ H3T 2B2, Canada.

Manuscript submitted February 22, 2011.
Article published online November 10, 2011

welded by using a linear friction welding process development system (PDS) at the Aerospace Manufacturing Technology Centre of the Institute for Aerospace Research, National Research Council (NRC) of Canada. During welding, the direction [001] was oriented perpendicular to the welding direction, *X* (Figure 1). The frequency and amplitude of oscillation during welding were 100 Hz and 2 mm, respectively. A compressive stress of 90 MPa was imposed on the material at the forging phase of the welding process. A total axial shortening of approximately 1.75 mm was achieved after a welding time of about 22 seconds. In order to study and analyze the effect of rapid thermal cycle and imposed compressive stress during joining, physical simulation of the LFW process was performed by using a Gleeble 1500-D thermo-mechanical simulation system (Dynamic System Inc, Poestenkill, NY). Specimens simulated to study the effect of thermal cycle alone, without imposed stress, were heated at a fast heating rate of 150 °C/s to temperatures ranging from 1373 K to 1623 K (1100 °C to 1350 °C) and held for specific holding times to a maximum of 2.5 seconds before air cooling. Specimens used to study the coupled effect of thermal cycle and imposed compressive stresses were heated to the peak temperatures, while the holding times and the percent length reductions at the peak temperatures were varied. As-cast, welded, and Gleeble-simulated specimens were sectioned, prepared by standard metallographic techniques for microstructural examination, and etched electrolytically in 12 mL H_3PO_4 + 40 mL HNO_3 + 48 mL H_2SO_4 solution at 6 V for 5 seconds. This etching procedure was used for other nickel-base superalloys.[8,9]

Microstructures of the specimens were examined and analyzed by a Zeiss Axiovert 25 (Carl Zeiss, Jena, Germany) inverted reflected-light optical microscope equipped with a Clemex vision 3.0 image analyzer (Clemex Technologies Inc., Longueuil, Quebec, Canada) and a JEOL* JSM 5900 scanning electron microscope (SEM) equipped with an Oxford (Oxford Instruments, Oxford, United Kingdom) ultrathin window energy-dispersive spectrometer (EDS) and Inca analyzing software (Oxford Instruments, Oxfordshire, UK). Selected welded specimens were chemomechanically polished by using colloidal silica solution to a surface finish of about 0.05 μm. Grain boundaries across the weld joint in these specimens were examined by carrying out electron backscatter diffraction (EBSD) based orientation mapping using an HKL Nordlys EBSD detector (developed by Oxford Instruments), which was attached to a PHILIPS** XL 30 SEM. The EBSD detector was equipped with the Oxford Instrument HKL Technology Channel 5 suite of programs. The orientation mapping was carried out at a step size of 1.5 μm. Unique grains having misorientations greater than 10 deg were represented in random grain colors, while special grain boundaries ($3 \le \Sigma \le 29$) were characterized based on the coincident site lattice (CSL) model.

*JEOL is a trademark of Japan Electron Optics Ltd., Tokyo.

**PHILIPS is a trademark of FEI Company, Hillsboro, OR.

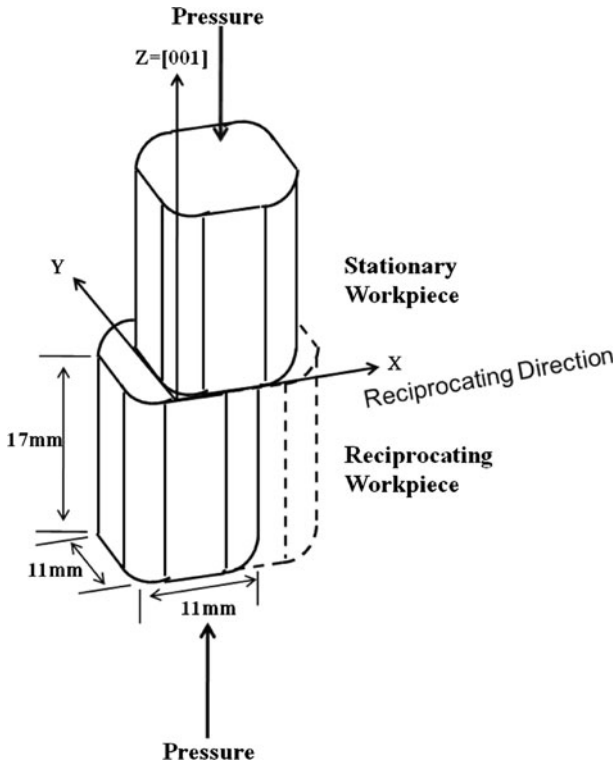

Fig. 1—Schematic representation of the specimen geometry and orientation during LFW of CMSX 486 superalloy.

III. RESULTS AND DISCUSSION

A. *Microstructure of Preweld Material*

The as-cast CMSX 486 superalloy has a directionally solidified columnar microstructure, as shown in the optical micrograph of Figure 2(a). The alloy typically consists of a regular distribution of ordered γ' precipitates that have an "ogdoadically diced cube" shape (clusters of cube particles[10]) and γ-γ' eutectic along the interdendritic regions (Figure 2(b)). SEM examination also revealed the existence of block-shaped carbide particles distributed along the interdendritic regions (Figure 2(b)). Previous studies by transmission electron microscopy analysis of these carbide particles, extracted on carbon replicas, showed that they are Hf- and Ta-rich MC-type carbides with an fcc crystal structure and lattice parameter of 0.465 nm.[3] Aside from γ-γ' eutectic and MC-type carbides, a careful SEM study revealed the occurrence of a different eutectic-like microconstituent ahead of some of the γ-γ' eutectic (Figure 2(c)). A major constituent of the eutectic-like product is a nickel-base phase that is relatively rich in Hf compared to the γ matrix phase (Figure 2(c) and Table I). Hafnium is known to selectively partition into interdendritic liquid

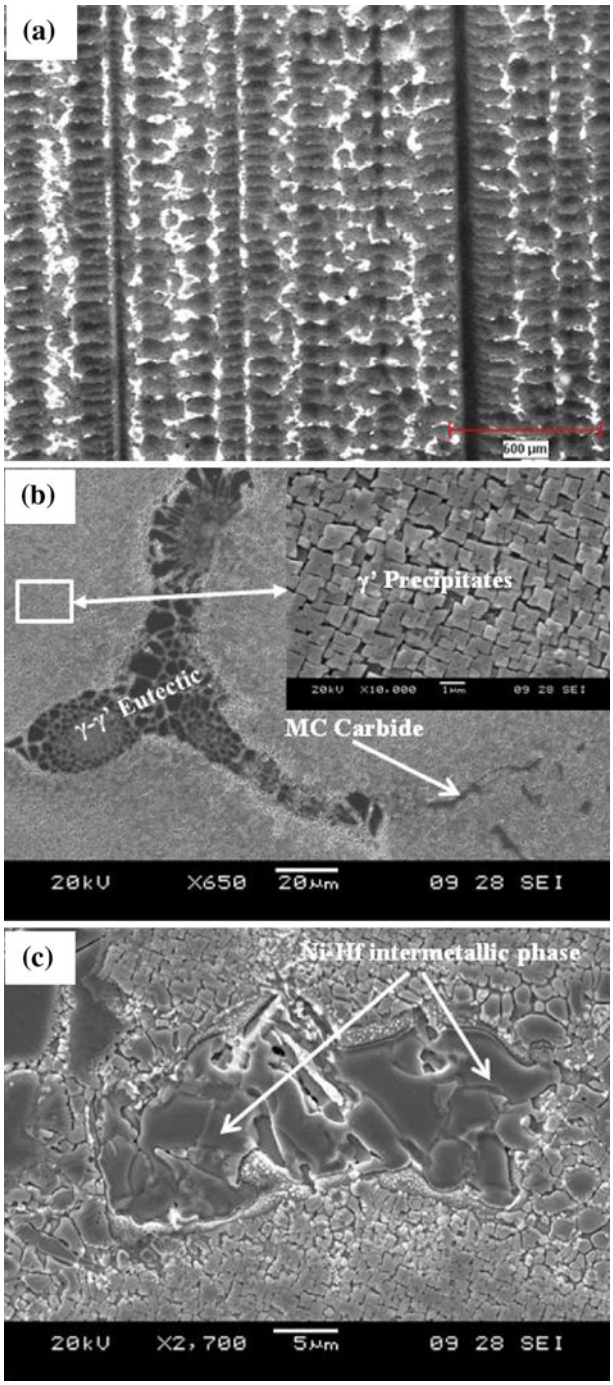

Fig. 2—(*a*) Low-magnification optical micrograph showing the columnar dendritic structure of CMSX 486 superalloy. (*b*) SEM micrograph illustrating MC type carbides, γ-γ' eutectic, and γ' precipitates. (*c*) SEM micrograph showing Ni-Hf intermetallic phase in the as-cast material.

Table I. Chemical Composition of Ni-Hf Intermetallic Phase in As-Cast CMSX 486 Superalloy

Element	Ni	Al	Co	Hf	Cr	Ti
At. pct	67.66	15.61	6.81	6.33	2.35	1.25

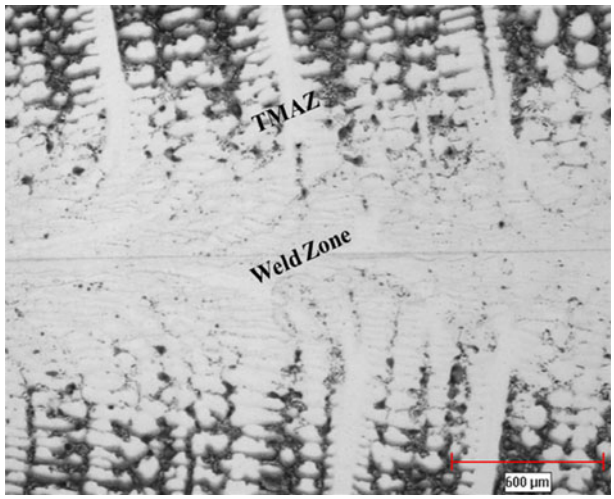

Fig. 3—Optical micrograph showing an overview of the linear friction welded joint in CMSX 486 superalloy.

during solidification of nickel-base superalloys, including the present alloy CMSX-486.[3] This microsegregation behavior of Hf was reported to result in formation of Ni-Hf intermetallic phase by a eutectic-type terminal solidification reaction in front of γ-γ' eutectic in other nickel-base superalloys.[11,12]

B. *Microstructure of Welded Material*

A general overview of the weld area revealed two distinct microstructural regions across the weld, the weld zone (WZ) and the thermomechanically affected zone (TMAZ), as illustrated by the optical micrograph presented in Figure 3. Higher magnification examination of these regions under SEM showed that they are free of cracks. The WZ, formed between the two workpieces, extended to about 250 μm, and γ' precipitates, γ-γ' eutectic, and the Hf-rich nickel-base phase completely dissolved within this zone while the MC carbides exhibited partial dissolution (Figures 4(a) through (c)). In the TMAZ, however, which formed beyond 250 μm from the weld line into the base material, only the Hf-rich nickel-base phase was observed to have completely dissolved, while the other second-phase particles exhibited limited dissolution (Figures 5(a) and (b)).

A notable microstructural event that is not generally expected during LFW is significant melting. The joining process was generally considered, like other friction welding processes, to be an exclusively solid-state joining technology.[13,14] However, in the present work, significant melting involving liquation reactions of secondary phases was observed to have occurred in the linear friction welded CMSX-486 superalloy. Figure 6(a) is a low-magnification micrograph of a liquated interdendritic region in the TMAZ, and a higher magnification micrograph that shows resolidified fine eutectic product in this region is presented in Figure 6(b). A careful microstructural analysis of the welded joint also revealed that, while the WZ and TMAZ were crack free, a continuous Hf-base oxide film was formed on a significant portion of the weld line, as

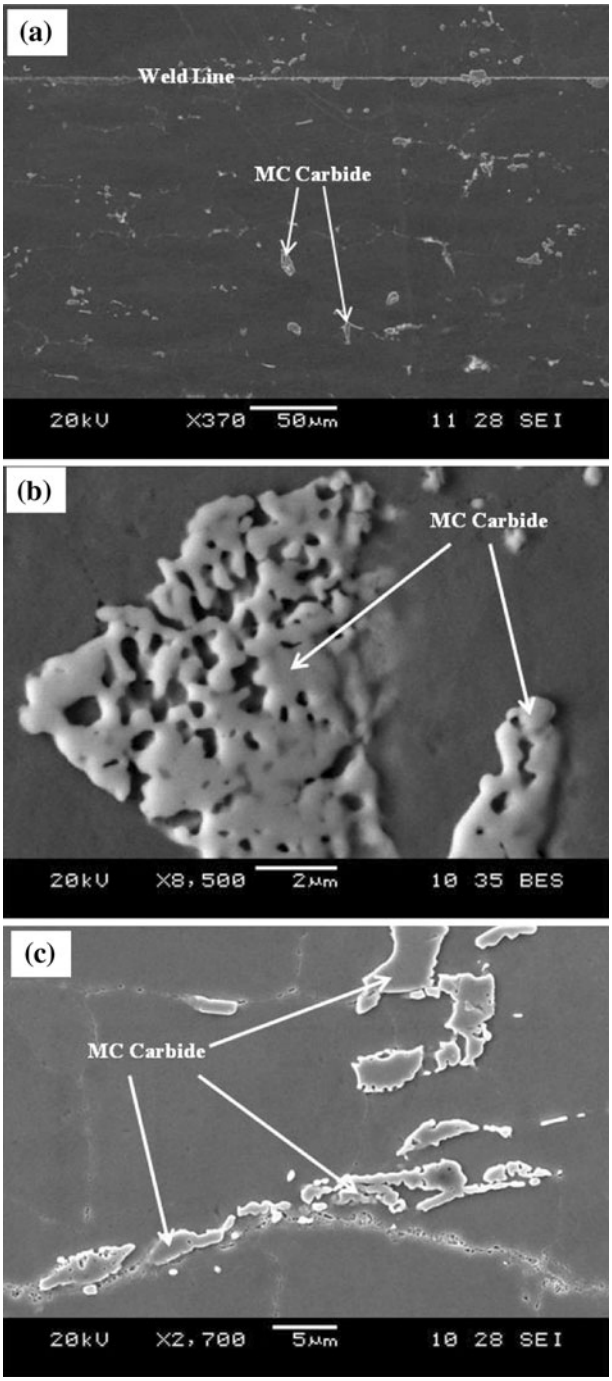

Fig. 4—SEM micrographs showing (*a*) an overview of the WZ and (*b*) and (*c*) MC carbides in the WZ.

shown in Figures 7(a) and (b). SEM-EDS qualitative microchemical analysis showed that the phase contains significant concentration of oxygen (Figure 8), but oxygen was not quantified due to the limitation of the technique in quantifying light elements with sufficient accuracy. Nonetheless, semiquantitative EDS analysis of the metallic component of the oxide phase showed that the Hf content of the oxide phase was more than 70 at. pct (Table II). As mentioned earlier, liquation occurred during LFW of CMSX 486. In order to study

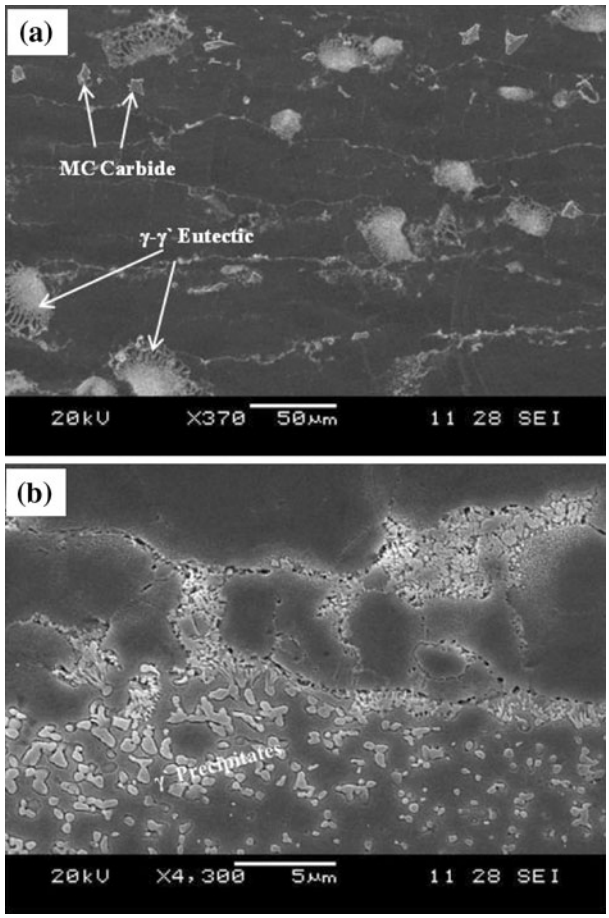

Fig. 5—SEM micrographs showing (*a*) an overview of the TMAZ and (*b*) partially dissolved γ' precipitates in the TMAZ.

and analyze microstructural development during welding, Gleeble simulation of the welding process was performed. The result of this investigation will be presented in Section III–C.

C. *Liquation of Various Phases in CMSX 486 Superalloy*

Specimens of CMSX-486 superalloy were rapidly heated by the Gleeble system to temperatures ranging from 1373 K to 1623 K (1100 °C to 1350 °C), followed by air cooling, to investigate the effect of rapid thermal cycle during welding on the microstructure of the alloy. Significant occurrence of liquation was observed in the specimens that were heated to peak temperatures from 1423 K to 1623 K (1150 °C to 1350 °C). The initial observation of liquation was made at 1423 K (1150 °C), in interdendritic locations that previously contained the Hf-rich nickel-base phase that formed in front of the γ-γ' eutectic in the as-cast material. The interdendritic liquated areas, as observed at all temperatures above 1423 K (1150 °C), contained newly formed fine eutectic product that consisted of a major phase that chemically appeared to be based on Ni_5Hf intermetallic[12,15] (Figures 9(a) and (b), and Table III). Incipient melting due to γ-Ni_5Hf eutectic reaction was reported to occur in a Hf-bearing nickel-base superalloy at temperatures around 1423 K (1150 °C). A similar type of resolidified

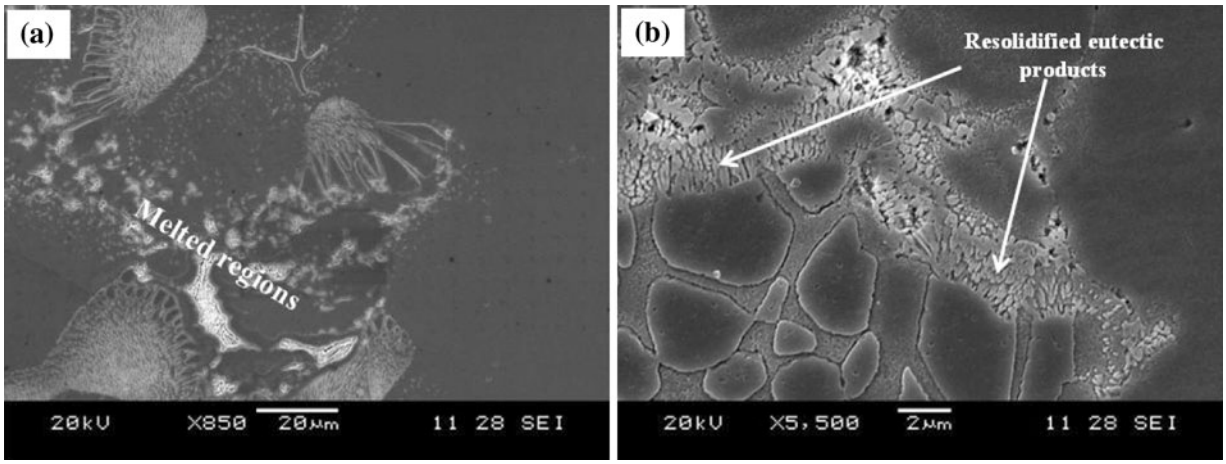

Fig. 6—SEM micrographs of linear friction welded CMSX 486 superalloy showing (*a*) liquation in the interdendritic region and (*b*) resolidified γ-γ' eutectic products.

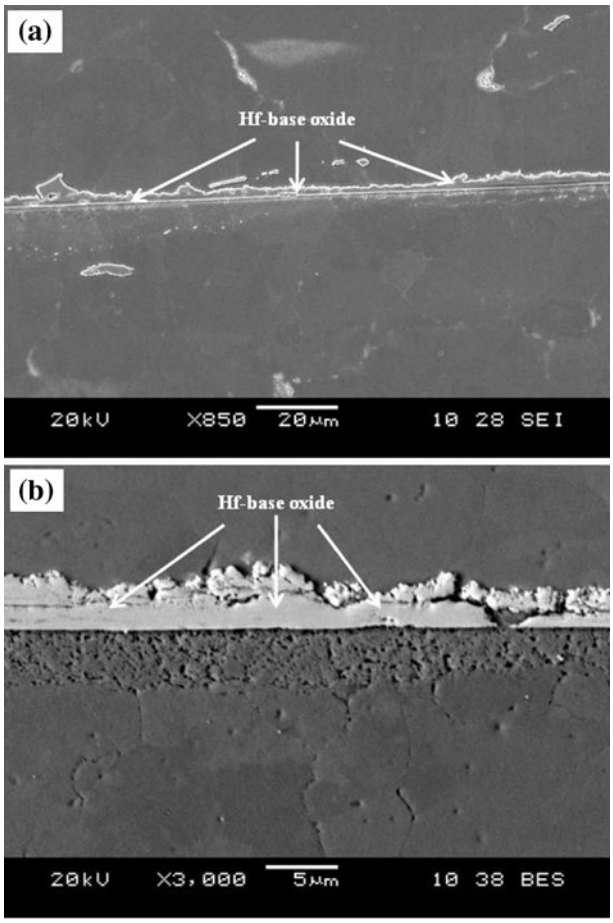

Fig. 7—SEM micrographs of the weld line showing Hf-base oxide layers.

fine eutectic microconstituent was observed in TMAZ interdendritic regions of actual linear friction welded material, including a phase with morphology and chemical composition similar to the Ni-HF phase observed in the liquated areas in Gleeble-simulated material (Figure 9(c) and Table III).

Aside from the melting that was apparently caused by the liquation reaction of the Hf-rich nickel-base phase in the alloy, with a further increase in peak temperature to above 1548 K (1275 °C), the main strengthening phase of the alloy, γ' precipitates were also observed to liquate through a phenomenon known as constitutional liquation. Constitutional liquation of second-phase particles was first proposed by Pepe and Savage,[16] and it was observed by different investigators in various alloy systems.[16–18] It occurs generally below an alloy's equilibrium solidus temperature by a eutectic-type reaction between a second-phase particle and the surrounding matrix, producing a metastable solute-rich liquid film at the particle/matrix interface. The basic requirement for the occurrence of constitutional liquation of an intermetallic compound A_xB_y in an alloy is the existence of A_xB_y particle at temperatures equal to or above the eutectic temperature of the matrix-A_xB_y system.[16] It is generally known that γ-γ' eutectic reaction occurs during solidification of several γ' precipitation-hardened nickel-base superalloys. The γ-γ' eutectic reaction is often assumed to occur at the solidus temperature as final solidification reaction during casting of the alloys. Ni-Al-Cr and Ni-Al-Ti are the two ternary systems mostly used to represent γ' precipitation-hardened nickel-base superalloys. The phase configuration for Ni-Al-Ti alloys with low Ti concentrations is similar to that of the Ni-Al-Cr system.[19] Therefore, from a more theoretical point of view, the Ni-Al-Ti system is a good reference for the discussion of γ-γ' equilibria and the solidification path for γ' strengthened superalloys. Willemin and Durrand-Charre[20] studied liquid-solid equilibria in the nickel-rich corner of the Ni-Al-Ti system and have proposed a projection of the liquid surface for this system. According to the Ni-Al-Ti ternary system data, the eutectic reaction between γ and γ' phases is found to be noninvariant in nature. This implies that the γ-γ' eutectic reaction in the nickel superalloys based on this system occurs over a range of temperatures, and this was experimentally confirmed in a number of nickel-base superalloys.[21–23] Hence, there exists a temperature range in γ' precipitation-hardened

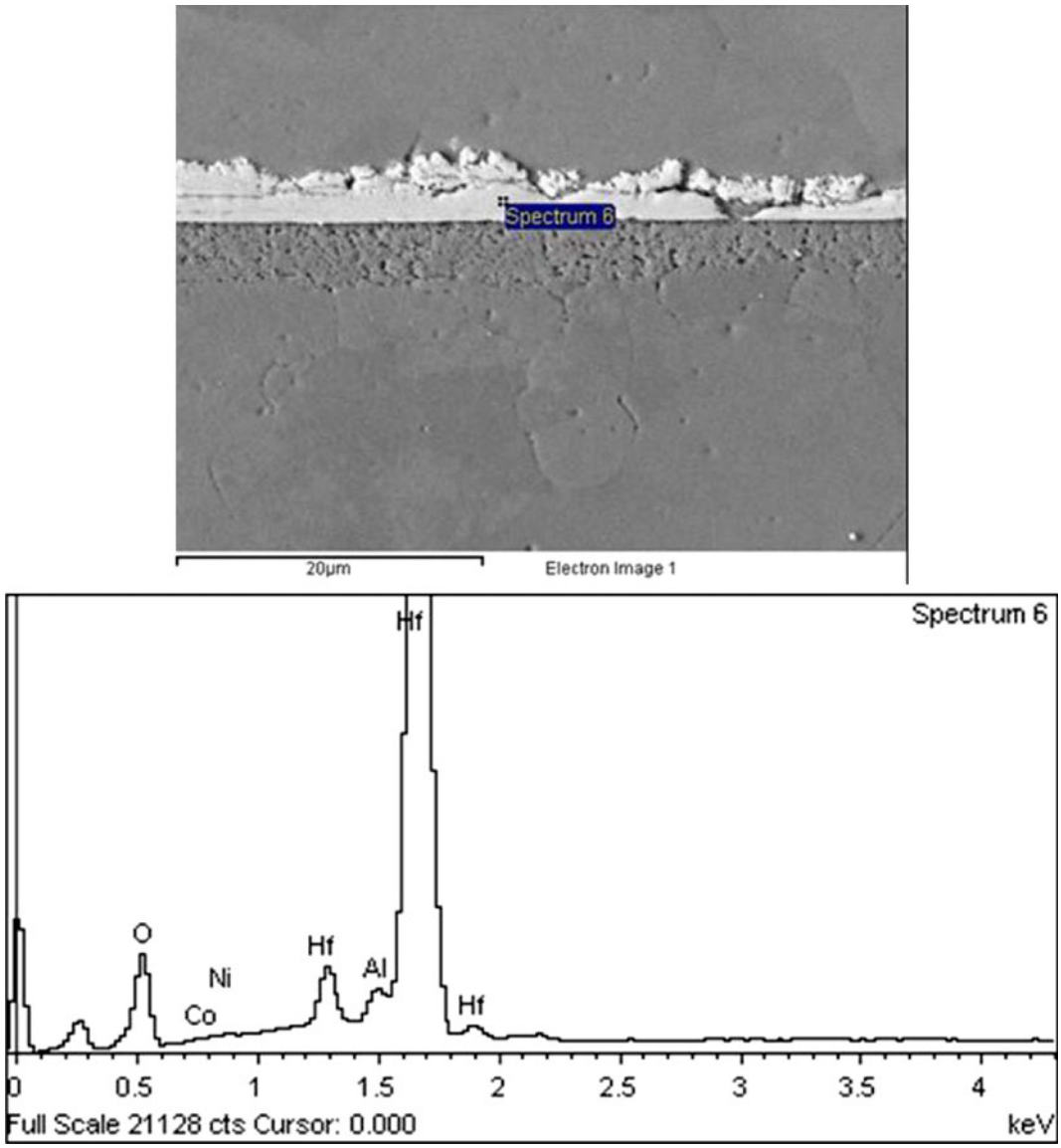

Fig. 8—EDS spectrum of Hf-base oxide on the weld line.

Table II. Chemical Composition of Hf-Base Oxide Layer in the Welded Material

Element	Ni	Al	Co	Hf
Wt pct	4.43	1.64	0.90	93.03
At. pct	11.22	9.02	2.28	77.48

Table III. Chemical Composition of Resolidified γ-Ni_5Hf Eutectic Phase in Gleeble-Simulated [at 1523 K (1250 °C)] and Welded Materials

Element	Ni	Al	Co	Hf	Cr
At. pct (Gleeble)	66.01	3.06	8.63	19.52	2.78
At. pct (Weld)	65.97	2.78	9.00	19.38	2.87

nickel-based alloys, within which γ-γ' eutectic reaction occurs and persistence of γ' particles to this temperature range during rapid heating could result in their constitutional liquation through γ-γ' eutectic-type reaction. The equilibrium solidus temperature of CMSX-486 was reported to be around 1561 K (1288 °C), as determined by differential scanning calorimetry,[3] but the temperatures at which γ-γ' eutectic reaction occurs in the alloy may extend below this value, due to the inherent sensitivity limitation of technique to solidification of low volume fraction of liquid phase, similar to the case in the IN738 superalloy.[24]

The Gleeble simulation experiments in the present work showed that some γ' precipitates in alloy CMSX-486 survived during rapid heating to temperatures up to 1573 K (1300 °C). Persistence of the γ' precipitates to temperatures above 1523 K (1250 °C), where γ-γ' eutectic reaction is possible, was observed to result not only in constitutional liquation of the particles, but also eutectic melting of pre-existing interdendritic γ-γ' eutectic (Figures 10(a) through (c)). A recent study was reported to show that the peak temperature within

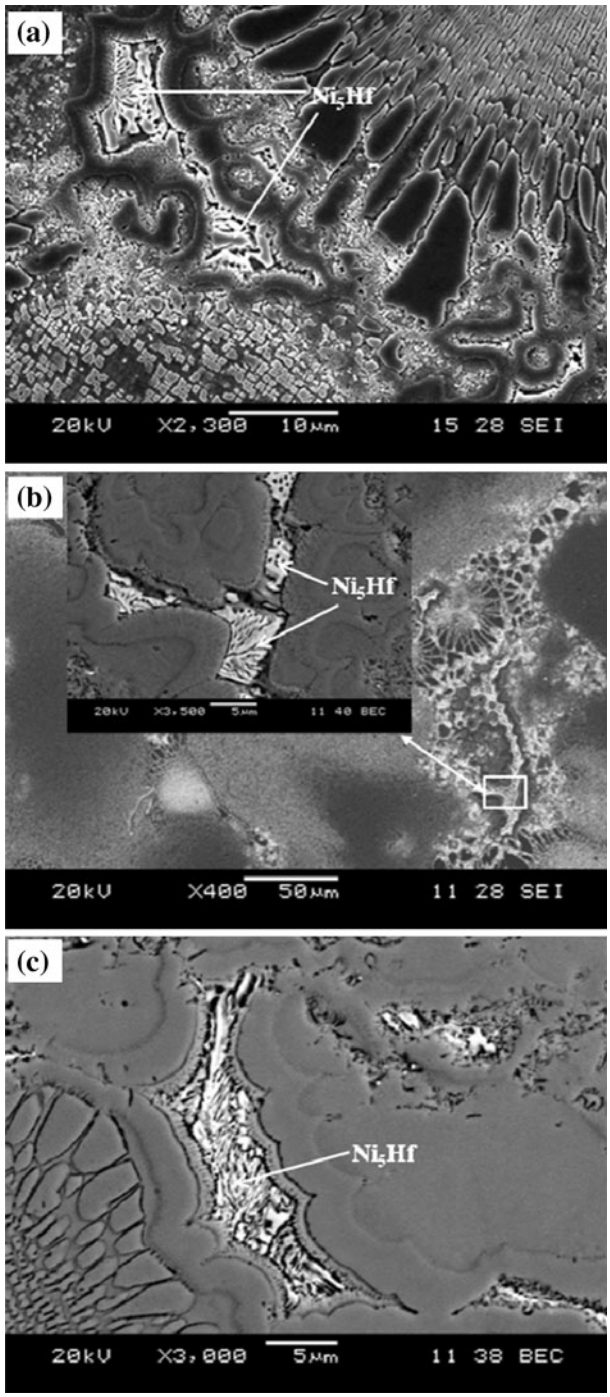

Fig. 9—SEM micrographs illustrating (*a*) and (*b*) liquation in the interdendritic regions of Gleeble-simulated materials rapidly heated to 1448 K (1175 °C) and 1523 K (1250 °C), respectively, and held for 0.5 s. (*c*) Welded material, showing γ-Ni_5Hf eutectic microconstituents.

the WZ during friction processing of alloys can be up to 0.97 T_m, where T_m is the melting temperature.[25] The equilibrium liquidus temperature of alloy CMSX-486 was reported to be around 1659 (1386 °C),[3] and, as such, the peak temperatures experienced by the alloy in the TMAZ during LFW can be expected to be up to the γ-γ' eutectic transformation temperatures in the alloy. The γ-γ' eutectic-type liquation reaction that occurred in the Gleeble-simulated specimens was also observed in the actual linear friction welded CMSX-486 material (Figure 10(d)).

Although good correlations exist between the microstructure of the Gleeble thermally cycled specimens and that of the actual linear friction welded material, in terms of the liquation reaction of second-phase particles, an important discrepancy between them was observed with regard to the increase in the formation of resolidified eutectic products with peak temperature. The Gleeble thermomechanical simulation results showed that an increase in peak temperature resulted in more liquation and a larger extent of formation of concomitant resolidified eutectic products, as illustrated in Figures 11(a) and (b) for peak temperatures of 1498 K and 1548 K (1225 °C and 1275 °C), respectively. In contrast, however, the formation of resolidified eutectic products considerably reduced with the increase in peak temperature from the TMAZ to WZ in the linear friction welded material, to the extent that no resolidified fine γ-γ' eutectic or those containing the Ni-Hf intermetallic phase were observed in the WZ (Figure 4(a)). This is also at variance with what is typically observed in conventionally welded materials, in that formation of resolidified eutectic products normally increases from the HAZ toward the weld fusion zone. Knowing that during LFW the material did not only experience higher temperature, but also mechanical strain caused by imposed forging compressive load, proper understanding of the WZ microstructure may not be possible without considering the effect of the applied compressive stress during joining, and this is discussed in Section III–D.

D. *Effect of External Compressive Stress on Weld Microstructure*

One primary way by which metastable liquid formed by the liquation of second-phase particles resolidify is through solid-state back-diffusion of solute atoms away from the liquid phase into the surrounding solid matrix.[26,27] The solid-state diffusion flux, J, of a solute is dependent on the chemical potential gradient of the solute, μ, and it is represented by

$$J = -MC\frac{d\mu}{dx} \qquad [1]$$

where M is the atomic mobility, C is the solute concentration, and $d\mu/dx$ is the chemical potential gradient. The chemical potential gradient is the major driving force for atomic diffusion, and any factor that increases it will normally enhance diffusion. The main parameter that is often used to represent the chemical potential gradient and to discuss diffusion behavior in alloys is the solute concentration gradient. Nevertheless, besides the commonly used concentration gradient, there are other parameters that can contribute to the overall gradient of chemical potential of a solute in a material, and these include the strain gradient and electrical potential gradient.[28] During LFW, the

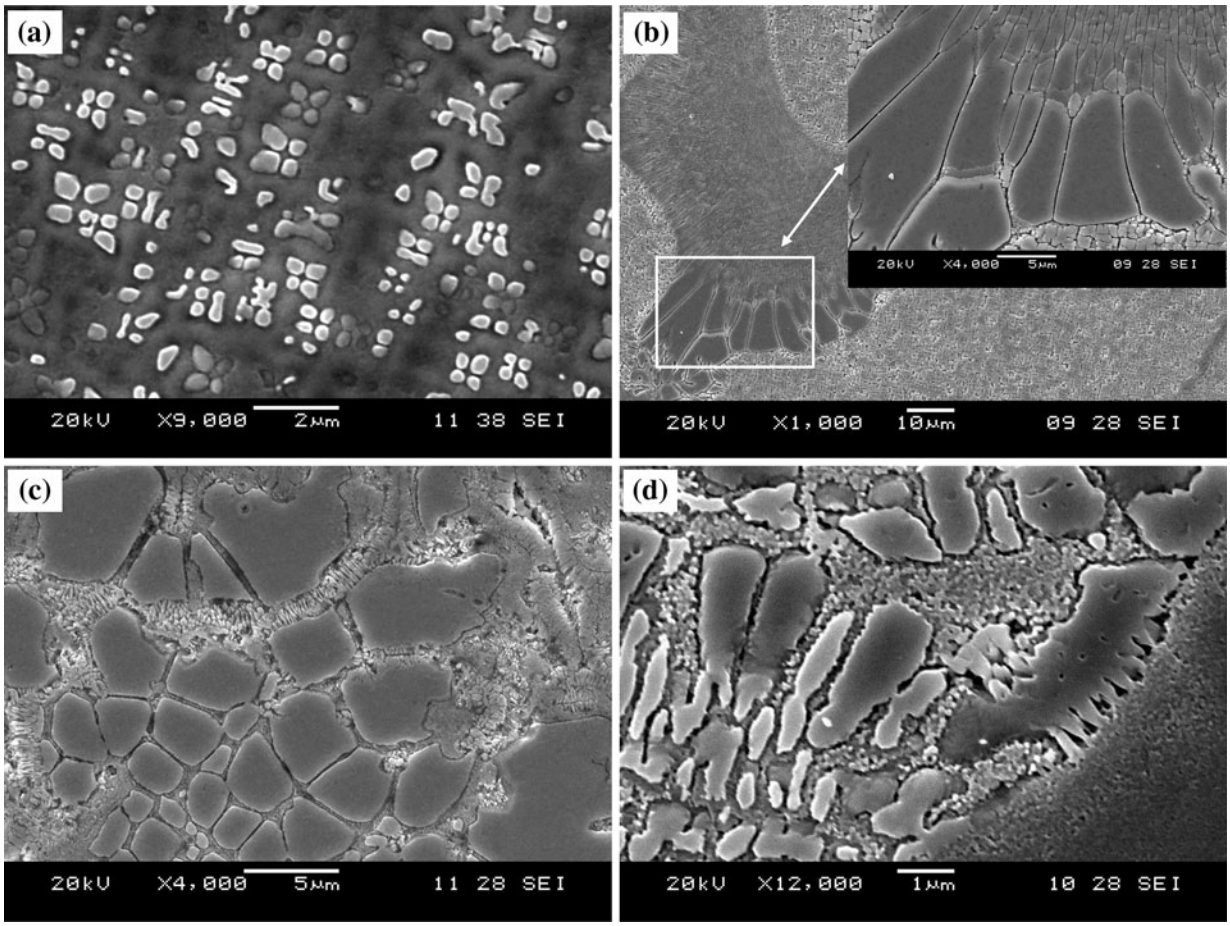

Fig. 10—SEM micrographs showing (*a*) γ' precipitates in a Gleeble material rapidly heated to 1523 K (1250 °C) and held for 0.5 s, (*b*) γ-γ' eutectic in the as-cast material, (*c*) liquating γ-γ' eutectic in a Gleeble material at 1523 K (1250 °C), and (*d*) liquating γ-γ' eutectic in the TMAZ of the welded material.

imposed forging compressive stress normally produces a strain gradient in work pieces being joined due to the existence of temperature variation from the WZ to TMAZ and the base material. The induced strain gradient could augment the driving force for atomic diffusion through its positive contribution to the overall chemical potential gradient. Furthermore, aside from the possible contribution to the chemical potential gradient, the externally applied compressive stress can enhance diffusion through its influence on the magnitude of the atomic mobility, M, in Eq. [1]. The value of M is given by the Nernst–Einstein equation as

$$M = \frac{D}{\mathrm{k}T} \qquad [2]$$

where k is the gas constant; T is the absolute temperature; and D is the diffusion coefficient, which is dependent on the activation energy for diffusion. Even though it is not commonly discussed, the activation energy for diffusion can be influenced by mechanical strain experienced by a solid. Through a rigorous and meticulous analytical study of vacancy-assisted atomic diffusion, a relationship between activation energy per unit strain, Q', and diffusion coefficient under strain, D (strain), and without strain, D (relax), was given by[29]

$$D(\text{strain}) = D(\text{relax}) \exp\left(\frac{-Q's}{\mathrm{k}T}\right) \qquad [3]$$

where s is the strain (negative for compression and positive for tension), k is a constant, and T is the absolute temperature. It can be seen from Eq. [3] that atomic diffusion can be enhanced by compressive strain, which has been experimentally confirmed in different alloy systems.[30,31] Additionally, an increase in dissolution of γ' precipitates, which is typically known to be controlled by diffusion of γ'-forming elements away from the precipitate/matrix interface, was observed to be significantly enhanced by externally induced compressive strain in a nickel-base Nimonic 115 superalloy (Special Metals Corporation, Huntington, WV).[32] A similar observation of increased second-phase particle dissolution under compressive strain was reported in another nickel-base superalloy.[33] These indicate that strain-enhanced diffusion occurs in nickel-base superalloys. Consequently, it is conceivable that the strain generated by the imposed compressive stress during LFW can aid the resolidification of the metastable liquid phase produced during joining through the enhanced solute back-diffusion process. This possibility was investigated in the present work by studying and comparing

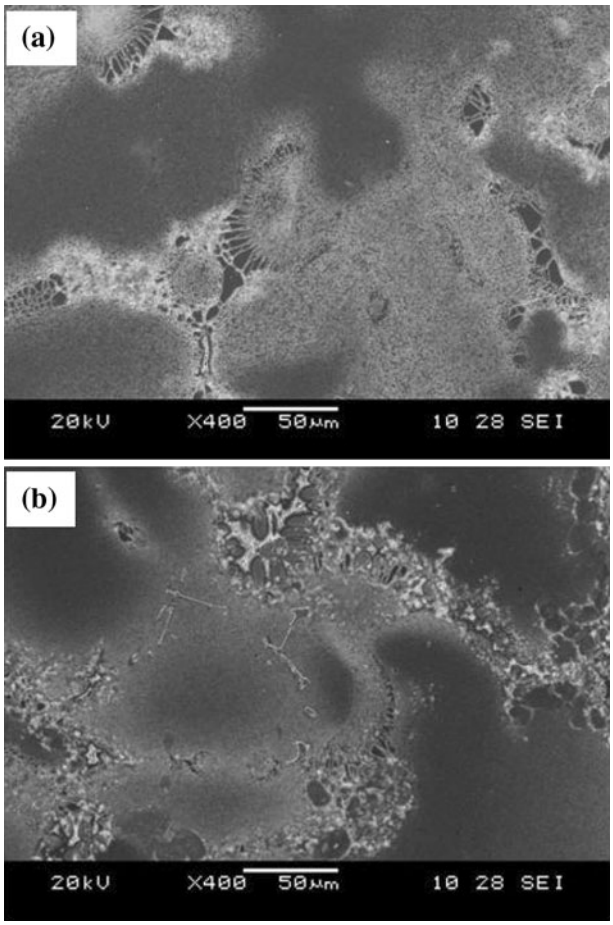

Fig. 11—SEM micrographs of Gleeble-simulated materials rapidly heated to (*a*) 1498 K (1225 °C) and (*b*) 1548 K (1275 °C), held for 0.5 s.

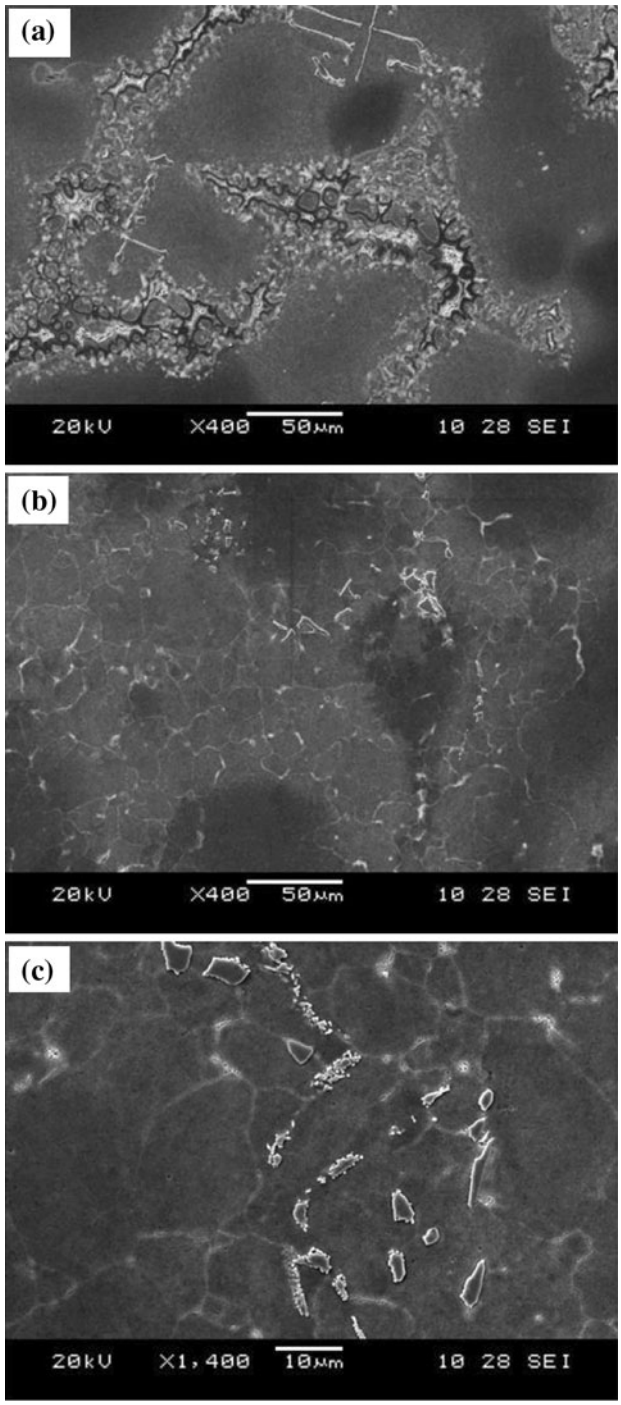

Fig. 12—SEM micrographs of Gleeble-simulated materials rapidly heated to 1548 K (1275 °C) and held for 2.5 s: (*a*) thermal cycle alone, (*b*) thermal cycle + 27 pct compressive strain at peak temperature, and (*c*) higher magnification of (b).

the extent of resolidification of the metastable liquid produced by the nonequilibrium liquation reaction of second-phase particles in CMSX-486 exclusively under thermal environment and under thermal environment plus imposed compressive strain, using the Gleeble system. The results showed that while extensive resolidified eutectic products were formed in specimens subjected to high temperatures without imposed stress, application of compressive stress at the peak temperatures, for the same holding time as those under thermal effect alone, produced remarkable reduction of the eutectic microconstituent (Figures 12(a) through (c)). The higher the magnitude of the applied strain, the greater was the extent of reduction of the resolidified eutectic product formation. This is attributable to the effect of imposed compressive strain in aiding resolidification of the metastable liquid through strain-enhanced solute back-diffusion during holding at the peak temperatures, thereby reducing or precluding residual liquid that transforms to eutectic products by nonequilibrium solidification reaction during cooling. A similar facilitating effect of imposed compressive stress on the resolidification process was observed and reported in another nickel-based superalloy IN 738.[7] Hence, preclusion of resolidified eutectic products in the WZ of the linear friction welded CMSX-486, which, as earlier stated, is at variance with what was observed in Gleeble-simulated specimens subjected to thermal cycle alone, can be explained by a more rapid resolidification of the liquid formed, enabled by the imposed strain in the WZ. Aside from the observation of a more rapid resolidification in the WZ, another important microstructural

feature was observed in the WZ, and this is discussed in Section III–E.

E. *EBSD-Based Orientation Mapping*

An important microstructural feature, which has been reported to occur during LFW of polycrystalline nickel-base superalloys,[12,34,35] is dynamic recrystallization, due to the thermomechanical condition imposed on the material during joining. In order to study the possible occurrence of recrystallized grains in the present welded alloy CMSX-486, the grain structure and character of grain boundaries in the WZ was studied by using EBSD based orientation mapping. The grain boundaries were characterized by studying an important grain boundary structural parameter, which was first proposed by Kronberg and Wilson,[36] termed the CSL. The EBSD mapping analysis revealed that recrystallized grains were formed in this region, as illustrated in Figure 13. Figures 13(a) and (b) show recrystallized grains in random colors on both sides of the weld line and the character of their grain boundaries, respectively. Most of the recrystallized grain boundaries had Σ values greater than 29 (Figure 13(b)), implying a very high degree of disorder.

The recrystallization behavior in the WZ of linear friction welded CMSX-486 was notable, in that finer (smaller) grains were present at the weld centerline area (Figures 13(a) and (b)) compared to other WZ areas away from the centerline, where the grains were more than 5 times greater. In the WZ, complete recrystallization of the grains was observed at both the weld centerline and adjacent WZ areas. It is known that there is a temperature range, ΔT, within which recrystallization and grain growth occur, and following complete recrystallization, a combination of high temperature and longer holding time within the ΔT normally aids the growth of newly

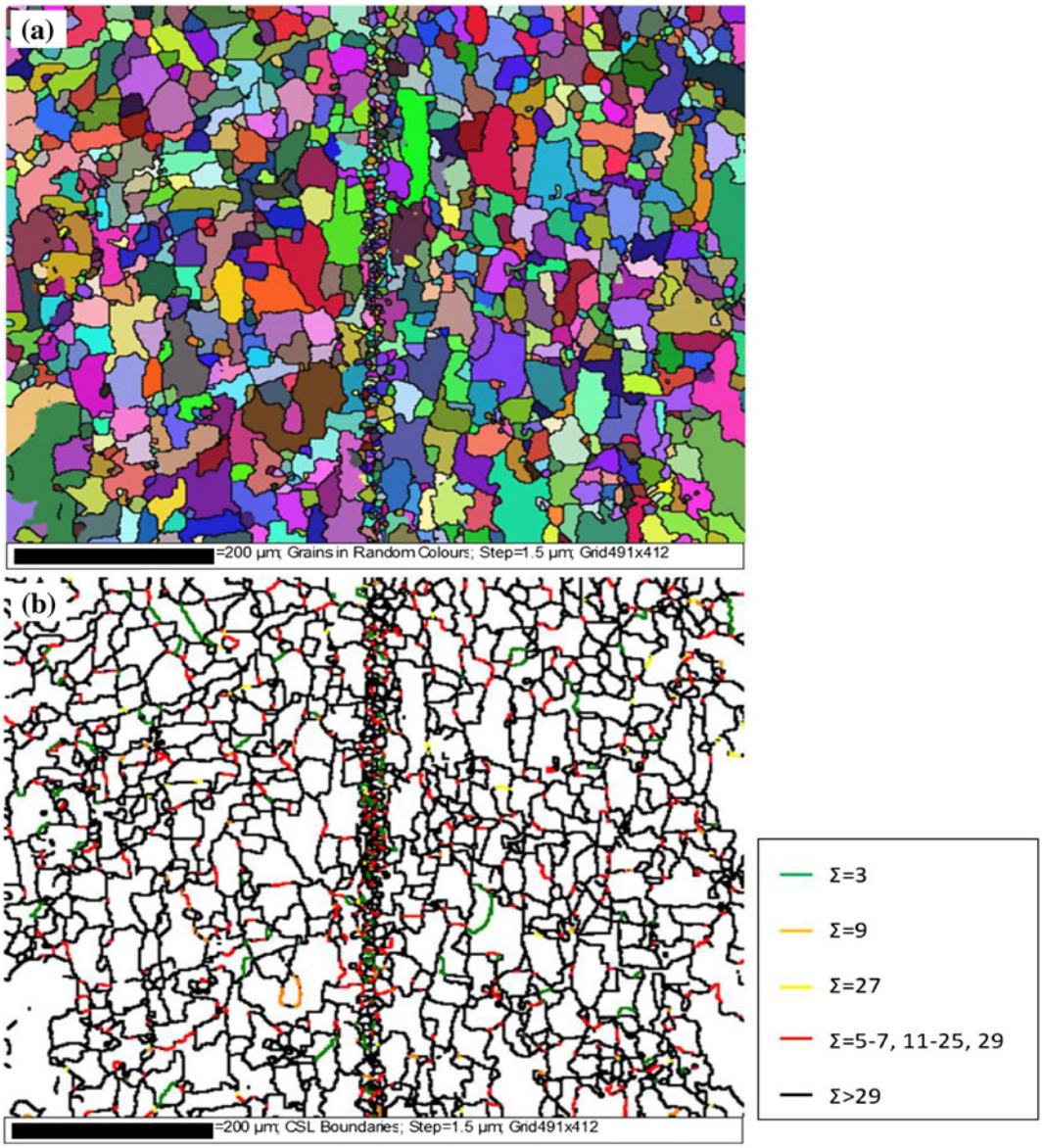

Fig. 13—EBSD-based orientation maps showing (*a*) the recrystallized grains in random colors across the weld centerline and (*b*) the character of the recrystallized grains (CSL boundaries), which is a map of Σ values.

formed fine grains to produce grains of larger size. The weld centerline area experienced the highest peak temperature during joining. Also, the joint area cools by the conduction of heat away from regions of higher temperature to regions of lower temperature in the base material. Therefore, it is reasonable to conceive that the weld centerline area, which experienced the highest temperature, spent a longer time within ΔT, compared to other WZ areas. Consequently, a larger grain size is expected at the weld centerline area of the WZ due to the fact that it experienced the highest temperature and longest time within ΔT. The formation of grains of larger sizes at the weld centerline, compared to other WZ areas, of friction welded materials were reported in the literature.[34,35] Therefore, the observation of smaller grains at the weld centerline area relative to other WZ areas in this present work is in contrast to the normally expected larger grains, which suggests that weld microstructure may not be solely explainable by classical solid-state recrystallization theory. The observed deviation from the expected behavior can be related to the liquation-resolidification processes that took place during joining. As previously stated, liquation occurred in these regions during joining. Since recrystallization is generally known to be a solid-state phenomenon, it is conceivable that recrystallization in the liquated regions would have occurred after complete solidification of the metastable liquid produced in these regions during the joining process. This implies that recrystallization may provide some information about the resolidification behavior in the material. In the region that solidified last, possibly due to the presence of more liquid, recrystallization might have commenced later compared to those regions that solidified earlier due to a relatively smaller amount of liquid. In such a situation, recrystallized grains in the weld centerline area can be smaller than those in other regions. Gleeble simulations showed that the extent of liquation increased with temperature. This implies that the highest amount of liquation would have occurred at the weld centerline area, due to this region being at the highest peak temperature, and this weld centerline area could have solidified last compared to other areas in the WZ. Hence, recrystallization could have started later at the weld centerline area and, thus, will have finer grains relative to other regions, as observed in the orientation maps. This observation, which does not seem to be explainable exclusively by solid-state reaction, is consistent with the observation of liquation of various phases and a more rapid solidification of the liquid due to imposed strain during linear friction welding, as reported and discussed in this work. Notwithstanding, a more rapid solidification and preclusion of resolidified eutectic products in the WZ, continuous Hf-base oxide film was observed along the weld line of the linear friction welded CMSX-486, and this is discussed in Section III–F.

Fig. 14—SEM micrograph of a Gleeble-simulated material rapidly heated to 1548 K (1275 °C) and held for 2.5 s.

F. *Oxidation of Hafnium-Rich Liquid in CMSX 486 Superalloy*

The nature of the oxide layer formed on the Gleeble-simulated specimens, which were processed under atmospheric condition, was carefully studied in order to gain an understanding of the formation of the Hf-base oxide film that was observed along the weld line in the linear friction welded material. Two main types of oxide scale, based on morphology and chemical composition, were observed on the specimens. The type 1 oxide scale consisted of a Ni-based oxide outer layer, and between

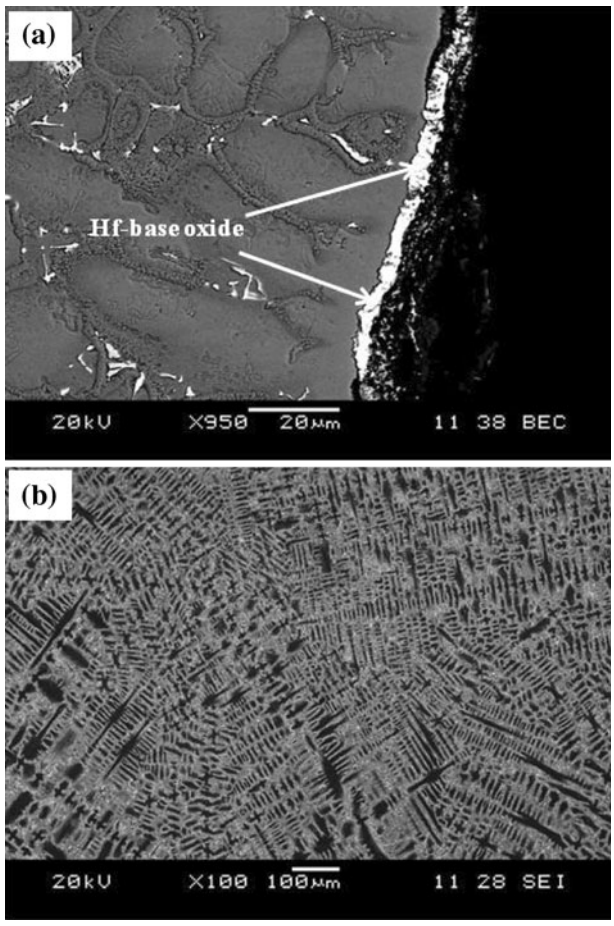

Fig. 15—SEM micrographs of a Gleeble-simulated material rapidly heated to 1623 K (1350 °C) and held for 0.5 s, showing (*a*) Hf-rich oxide and (*b*) a new dendritic structure.

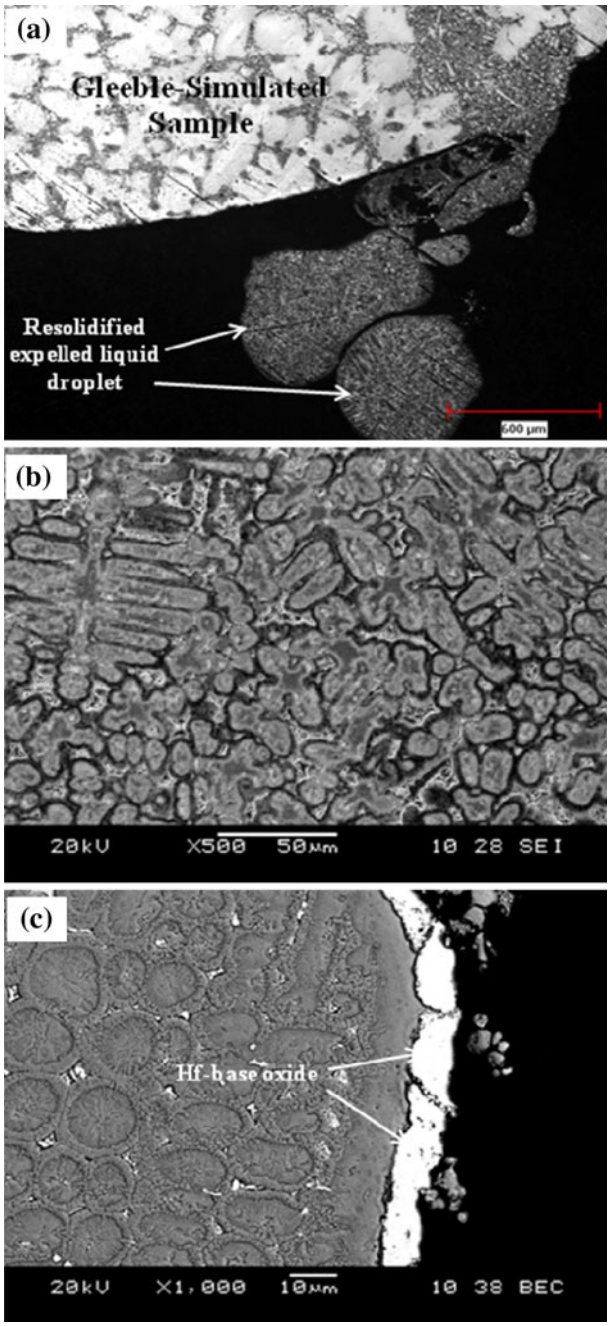

Fig. 16—SEM micrographs of a Gleeble-simulated material rapidly heated to 1548 K (1275 °C) and held for 2.5 s, with 27 pct strain at peak temperature, showing (*a*) resolidified expelled liquid droplet, (*b*) new dendritic structure of the resolidified liquid, and (*c*) Hf-base oxide layers on the liquid.

this top layer and the substrate alloy was a mixture of different oxide phases that were rich in Al, Cr, and Ni. The morphology of the type 1 oxide scale consisting of a mixture of the oxide phases is depicted by an atomic-number-based contrast in the SEM backscatter electron micrograph shown in Figure 14. Contrary to the multiphase oxides of type 1 oxide scale with different layers, the second type of oxide scale, type 2, essentially consisted of one layer of oxide phase, which was an Hf-base oxide, as shown in Figure 15.

Table IV. Chemical Composition of the Oxide Phase of Type 2 Morphology on the Liquid That Was Squeezed out of a Gleeble-Simulated Material at 1548 K (1275 °C)

Element	Ni	Al	Co	Hf	Cr
wt. pct	5.78	2.43	0.85	90.60	0.35
at. pct	13.72	12.55	2.01	70.78	0.95

The type 1 oxide scale was observed on the surface of all the Gleeble-simulated specimens and also on a CMSX-486 sample that was heated to 1573 K (1300 °C) in an ordinary laboratory furnace and held for 5 minutes in air. The type 2 oxide scale was only observed in those Gleeble specimens in which significant melting occurred during the rapid heating to high peak temperatures. One of these cases was at 1548 K (1275 °C), where application of compressive load on a Gleeble specimen resulted in squeezing out of interdendritic liquid phase (Figures 16(a) and (b)). The surface of the expelled liquid exposed to the atmosphere was subsequently oxidized to produce the type 2 oxide scale before the liquid became solidified (Figure 16(c) and Table IV). Likewise, at 1623 K (1350 °C), where significant bulk melting of the alloy occurred, type 2 oxide scale was observed on the exposed surface of melted regions, which resolidified with completely new dendritic microstructure (Figures 15(a) and (b)). A similar Hf-base oxide, suggested to be based on HfO_2 and with a metallic composition that is consistent with that of the type 2 oxide scale observed in this present work, was reported to form by oxidation of Hf-rich liquid during casting of a Hf-bearing nickel-base superalloy.[11]

One of the main reported technological merits of LFW is that it is generally considered as a "self-cleaning" process, where the oxides that are presumably formed in the solid state are broken down and extruded out of the joint region during the forging stage of joining.[37] In the present work, however, while the type 1 oxide scale was not observed in the linear friction welded CMSX-486, the continuous Hf-base oxide film that formed along the weld line was similar in morphology and composition to the type 2 oxide scale that was exclusively associated with liquation in Gleeble-simulated specimens. Therefore, even though the applied forging compressive load aided resolidification of liquid formed in the WZ during joining, as previously discussed, some of the liquid exposed to the atmosphere at the mating surfaces of the work pieces appeared to have reacted with oxygen to produce the continuous Hf-base oxide film along the weld line. Formation of continuous Hf-base oxide was reported to be detrimental to the mechanical properties of Hf-bearing nickel-base superalloys.[11,38] Consequently, the observed formation of a continuous Hf-base oxide film along the weld line of the linear friction welded CMSX-486 superalloy could conceivably be deleterious to the mechanical integrity of the weld joint. Any factor that can reduce or eliminate the formation of continuous Hf-base oxide film would improve the reliability of LFW for the joining of alloy CMSX-486 and possibly other Hf-containing nickel-base superalloys. Possible measures

that may be taken to reduce or eliminate the formation of continuous Hf-base oxide film during LFW of alloy CMSX-486 are suggested as follows.

(1) The load applied during the LFW of CMSX-486 could be increased. This may help in two ways. First, a higher forging pressure can aid faster resolidification of the liquid in the WZ and, thereby, prevent or minimize the amount of liquid available for oxidation. Second, a higher pressure during oscillation can enable more intimate contact between the workpieces, such that oxygen access to the mating surfaces is significantly reduced.
(2) If application of increased forging load is found ineffective, the use of a shielding gas to minimize oxygen access to the weld region during joining should be considered. This approach may also be applicable to other materials that contain alloying elements that are highly sensitive to liquid-phase oxidation.

IV. SUMMARY AND CONCLUSIONS

1. Linear friction welding produced a crack-free joint in the extremely difficult-to-weld SX nickel-base CMSX-486 superalloy.
2. In contrast to the general assumption that LFW occurs exclusively in the solid state, an extensive liquation, involving nonequilibrium liquation reactions of secondary phases that were present in the preweld alloy, occurred during joining.
3. Rapid resolidification of the nonequilibrium liquid phase, assisted by the compressive stress imposed during joining, resulted in a WZ microstructure that was essentially free of resolidified eutectic product, which is in contrast to what is normally obtained during conventional fusion welding processes.
4. Notwithstanding the rapid resolidification event, part of the liquid phase in the WZ appeared to have reacted with atmospheric oxygen to produce a continuous Hf-rich oxide film along the weld line, which may require further studies on how to prevent its occurrence.

ACKNOWLEDGMENTS

The authors acknowledge the financial support received from NSERC. The technical assistance of M. Guérin and E. Dalgaard for LFW of CMSX-486 is also greatly appreciated. One of the authors (OTO) is grateful to the University of Manitoba for the award of a Graduate Fellowship.

REFERENCES

1. K. Harris and J. Wahl: *Proc. 6th Int. Charles Parsons Turbine Conf.*, Dublin, Ireland, Sept. 16–18, 2003, Institute of Materials, Minerals and Mining, London, UK, 2003, pp. 687–701.
2. J. Wahl and K. Harris: *Proc. ASME Turbo Expo*, 2009, vol. 4, pp. 861–71.
3. Y.L. Wang, O.A. Ojo, R.G. Ding, and M.C. Chaturvedi: *Mater. Sci. Technol.*, 2009, vol. 25, pp. 68–75.
4. A. Hirose, D. Nakamura, H. Yanagawa, and K.F. Kobayashi: *Mater. Sci. Forum*, 2003, vols. 426–432, pp. 4007–12.
5. S. Katayama and M. Sakamoto: *ASM Conf. Proc.–Joining of Advanced and Specialty Materials*, Oct. 18–20, 2004, ASM International, Materials Park, OH, 2005, pp. 108–12.
6. J.M. Vitek, S.S. Babu, J.W. Park, and S.A. David: *Superalloys 2004*, TMS, Warrendale, PA, 2006, pp. 459–65.
7. O.T. Ola, O.A. Ojo, P. Wanjara, and M.C. Chaturvedi: *Philos. Mag. Lett.*, 2011, vol. 91, pp. 140–49.
8. O.A. Ojo, N.L. Richards, and M.C. Chaturvedi: *Scripta Mater.*, 2004, vol. 50, pp. 641–46.
9. J.D. Liu, T. Jin, N.R. Zhao, Z.H. Wang, X.F. Sun, H.R. Guan, and Z.Q. Hu: *Sci. Technol. Weld. Join.*, 2010, vol. 15, pp. 194–98.
10. J.H. Westbrook: *Z. Kristallogr*, 1958, vol. 110, pp. 21–29.
11. Z. Yunrong and L. Chenggong: *Superalloys 1988*, TMS, Warrendale, PA, 1998, pp. 475–84.
12. A. Baldan: *J. Mater. Sci.*, 1990, vol. 25, pp. 4341–48.
13. S.V. Lalam, G.M. Reddy, T. Mohandas, M. Kamaraj, and B.S. Murty: *Mater. Sci. Technol.*, 2009, vol. 25, pp. 851–61.
14. M. Karadge, P. Frankel, A. Steuwer, C. Lovell, S. Bray, P.J. Withers, and M. Preuss: *Joining of Advanced and Specialty Materials*, Materials Science and Technology (MS&T), 2006: Product Manufacturing, ASM International, Materials Park, OH, The American Ceramic Society, Westerville, OH, Association for Iron and Steel Technology, Warrendale, PA, The Minerals, Metals and Materials Society, Warrendale, PA, pp. 35–44.
15. W. Tillmann and E. Lugscheider: *Proc. Int. Conf. on the Joining of Materials JOM-7*, The European Institute for the Joining of Materials, Helsingør, Denmark, 1995, pp. 236–47.
16. J.J. Pepe and W.F. Savage: *Weld. J.*, 1967, vol. 46, pp. 411s–422s.
17. O.A. Ojo and M.C. Chaturvedi: *Mater. Sci. Eng. A*, 2005, vol. 403, pp. 77–86.
18. H.R. Zhang and O.A. Ojo: *Philos. Mag. Lett.*, 2009, vol. 89, pp. 787–94.
19. M. Durand-Charre: *The Microstructure of Superalloys*, Gordon and Breach Science Publishers, Amsterdam, Netherlands, 1997.
20. P. Willemin and M. Durrand-Charre: *J. Mater. Sci.*, 1990, vol. 25, pp. 168–74.
21. R. Rosenthal and D.R.F. West: *Mater. Sci. Technol.*, 1999, vol. 15, pp. 1387–94.
22. O.A. Ojo, N.L. Richards, and M.C. Chaturvedi: *J. Mater. Sci.*, 2004, vol. 39, pp. 7401–04.
23. R.K. Sidhu, O.A. Ojo, and M.C. Chaturvedi: *J. Mater. Sci.*, 2008, vol. 43, pp. 3612–17.
24. O.A. Ojo, N.L. Richards, and M.C. Chaturvedi: *Mater. Sci. Technol.*, 2004, vol. 20, pp. 1027–34.
25. S. Swaminathan, K. Oh-Ishi, A.P. Zhilyaev, C.B. Fuller, B. London, M.W. Mahoney, and T.R. Mcnelley: *Metall. Mater. Trans. A*, 2010, vol. 41A, pp. 631–40.
26. B. Radhakrishnan and R.G. Thompson: *Metall. Mater. Trans. A*, 1992, vol. 23A, pp. 1783–99.
27. S.W. Baker and G.R. Purdy: *Acta Mater.*, 1998, vol. 46, pp. 511–24.
28. R.W. Balluffi, S.M. Allen, and W.C. Carter: *Kinetics of Materials*, John Wiley and Sons, Inc., New York, NY, 2005, pp. 41–76.
29. N.E.B. Cowern, P.C. Zalm, P. Van der Sluis, D.J. Gravensteijn, and W.B. de Boer: *Phys. Rev. Lett.*, 1994, vol. 72, pp. 2585–88.
30. P. Kringhøj, A.N. Larsen, and S.Y. Shirayev: *Phys. Rev. Lett.*, 1996, vol. 76, pp. 3372–75.
31. M. Onishi and H. Miura: *Trans. JIM*, 1977, vol. 18, pp. 107–12.
32. D. Shahriari, M.H. Sadeghi, and A. Akbarzadeh: *Int. J. Adv. Manuf. Technol.*, 2009, vol. 45, pp. 841–50.
33. Y. Wang, W.Z. Shao, L. Zhen, and B.Y. Zhang: *Mater. Sci. Eng. A*, 2001, vol. 528, pp. 3218–27.
34. C. Mary and M. Jahazi: *Adv. Eng. Mater.*, 2008, vol. 10, pp. 573–78.
35. M. Preuss, J.W.L. Pang, P.J. Withers, and G.J. Baxter: *Metall. Mater. Trans. A*, 2002, vol. 33A, pp. 3215–25.
36. M.L. Kronberg and F.H. Wilson: *TMS-AIME*, 1949, vol. 185, pp. 501–14.
37. M.E. Nunn: *1st Int. Conf. on Innovation and Integration in Aerospace Sciences*, Queen's University, Belfast, Northern Ireland, United Kingdom, 2005.
38. T.M. Simpson, A.R. Price, P.F. Browning, and M.D. Fitzpatrick: *Advanced Technologies for Superalloy Affordability*, TMS, Warrendale, PA, 2000, pp. 277–86.